

TrimTokenator-LC: Towards Adaptive Visual Token Pruning for Large Multimodal Models with Long Contexts

Hao Zhang* Mengsi Lyu* Bo Huang Yulong Ao[†] Yonghua Lin[†]

Beijing Academy of Artificial Intelligence (BAAI)

Abstract

Large Multimodal Models (LMMs) have proven effective on various tasks. They typically encode visual inputs into Original Model sequences of tokens, which are then concatenated with textual tokens and jointly processed by the language model. However, the growing number of visual tokens greatly increases inference cost. Visual token pruning has emerged as a promising solution. However, existing methods often overlook scenarios involving long context inputs with multiple images. In this paper, we analyze the challenges of visual token pruning in long context, multi-image settings and introduce an adaptive pruning method tailored for such scenarios. We decompose redundancy into intra-image and inter-image components and quantify them through intra-image diversity and inter-image variation, which jointly guide dynamic budget allocation. Our approach consists of two stages. The intra-image stage allocates each image a content-aware token budget and greedily selects its most representative tokens. The inter-image stage performs global diversity filtering to form a candidate pool and then applies a Pareto selection procedure that balances diversity with text alignment. Extensive experiments show that our approach can reduce up to 80% of visual tokens while maintaining performance in long context settings.

1 Introduction

Large Multimodal Models (LMMs) (Bai et al., 2025; Team et al., 2025; Zhu et al., 2025; Liu et al., 2024a; Lin et al., 2023) have substantially extended the inferential reach of Large Language Models (LLMs) (Brown et al., 2020; Touvron et al., 2023; Chiang et al., 2023; Zhu et al., 2023; Li et al., 2023; Zhang et al., 2023; Huang et al., 2023; Wang et al., 2023) by enabling unified reasoning over heterogeneous inputs that combine vision and language. Standard pipelines first convert images into

Original Model visual token sequences via a vision encoder, after which these tokens are fused with textual tokens and processed jointly within a transformer backbone. Although this integration strategy supports strong multimodal understanding, it also produces exceptionally long sequences that often span several thousand tokens. The quadratic scaling behavior of attention with respect to sequence length (Vaswani et al., 2017; Face, 2024; Chen et al., 2023; Keles et al., 2023; Liu et al., 2022) yields substantial memory and computational overhead under such conditions. These costs present nontrivial barriers to deploying LMMs in practice, particularly in settings where inference latency or computational resources are tightly constrained (Chen et al., 2024a; Lin et al., 2025).

Recent studies indicate that visual tokens in LMMs is heavily overcomplete, with many visual embeddings contributing minimal semantic value to multimodal reasoning (Liu et al., 2024b; Shang et al., 2024; Huang et al., 2024; Tong et al., 2025; Li et al., 2025a). This observation has motivated a growing literature on strategies that selectively suppress redundant visual tokens during inference. Reducing the number of visual tokens shortens the multimodal sequence delivered to the transformer, which in turn mitigates the quadratic computational burden inherent in attention. A consistent finding across prior work is that substantial reductions in visual tokens can be achieved with only marginal impact on performance (Zhang et al., 2024a; Chen et al., 2024a; Lin et al., 2025; Huang et al., 2024; Sun et al.).

Existing visual token pruning methods can be broadly categorized into three types. (1) One prevalent direction leverages attention scores to identify redundant tokens and discard those with limited contribution (Lin et al., 2025; Shang et al., 2024; Tong et al., 2025). (2) Another class of methods introduces model-specific calibration or fine-tuning (Ye et al., 2025; Lin et al., 2025; Li et al., 2025b;

*These authors contribute equally to this work.

[†]Corresponding author.

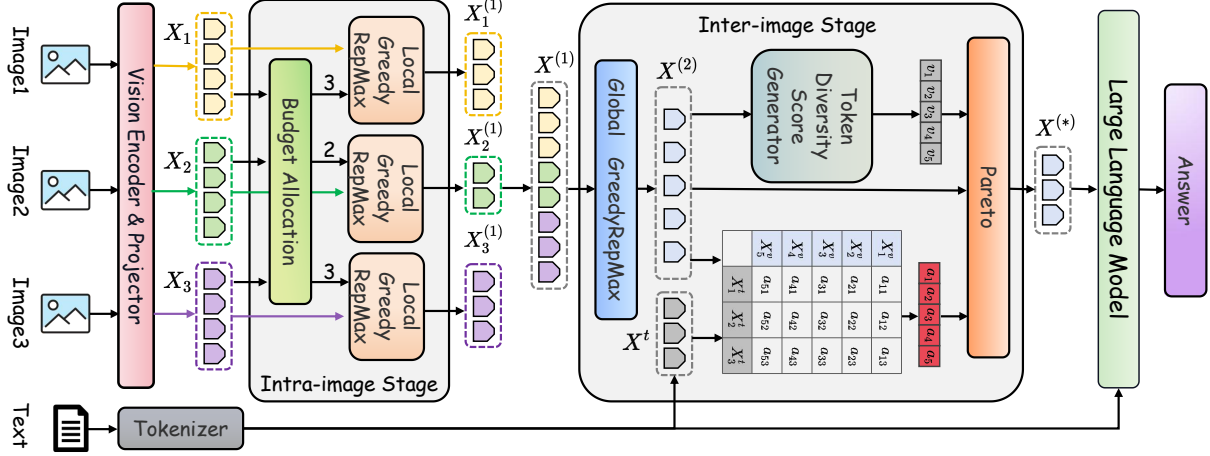


Figure 1: Comprehensive overview of the pruning method. We first perform an Intra-image Stage, where the visual token budget is adaptively allocated based on the diversity of each image. Within each image, a greedy representative selection strategy is applied to retain the most representative local visual tokens. Next, in the Inter-image Stage, greedy representative filtering is conducted over the candidate tokens collected from all images. Finally, by jointly considering token diversity and semantic alignment with the text, pareto selection is used to preserve tokens that are both informative across images and highly aligned with the text. Figure 2 provides a brief description.

Cai et al., 2024), which incurs substantial computational cost and restricts scalability in practical applications. (3) Another line of work emphasizes representation diversity and semantic relevance (Zhang et al., 2025a,b; Alvar et al., 2025; Li et al., 2025a), seeking to preserve tokens that carry the most informative content. However, all these methods largely overlook cases where the inputs involve long contexts. In such scenarios, the input sequence can be extremely long and often includes multiple images. Consequently, designing an effective token pruning strategy tailored to long context tasks becomes a considerably challenging problem.

In this paper, we analyze the challenges of visual token pruning in long context settings. Accordingly, we propose an adaptive visual token pruning method designed for multi-image long context scenarios. We categorize redundancy into intra-image and inter-image forms, and model these two aspects using intra-image diversity and inter-image variation. These measures guide the dynamic allocation of pruning budgets. Our method is composed of two procedures, intra-image pruning and inter-image pruning. The intra-image pruning procedure allocates different token budgets to each image based on its visual richness and employs a greedy strategy to select the most representative tokens, thereby yielding a compact representation for each image. The inter-image pruning procedure performs global diversity filtering over all image tokens to obtain a candidate set. It then applies

Pareto selection based on diversity and text alignment indicators to retain the tokens that contribute most across images and are most relevant to the textual context. These tokens form the final visual representation. Extensive experiments demonstrate that our method preserves strong performance in long context scenarios while substantially reducing the number of visual tokens. In summary, our contributions can be summarized as follows:

- We identify the key challenges of visual redundancy in long context settings and introduce an adaptive visual token pruning method for multi-image inputs, which allocates pruning budgets by modeling intra-image diversity and inter-image variation.
- We perform intra-image pruning by allocating per-image token budgets based on visual richness and using a greedy strategy to retain the most representative tokens, yielding compact visual representations.
- We conduct inter-image pruning by applying global diversity filtering over all image tokens to obtain a candidate set, and then use Pareto selection to retain the tokens that contribute most across images and most relevant to text.

2 Related Work

Visual Token Pruning aims to reduce computational cost and speed up inference by remov-

ing redundant or weakly informative visual tokens. **(1) One major line of research relies on attention statistics to estimate token importance.** PruMerge (Shang et al., 2024) merges clustered tokens in the vision encoder according to attention sparsity. FastV (Chen et al., 2024a) uses early attention signals to guide removal. SparseVLM (Zhang et al., 2024b) performs text conditioned token selection through cross modal attention, and VisionZip (Yang et al., 2025) compresses visual inputs based on CLS attention in the final vision encoder layer. FlowCut (Tong et al., 2025) identifies redundancy by tracing information flow across attention layers, while LVPPruning (Sun et al., 2025) measures importance from interactions between visual and language tokens. **(2) Another direction uses calibration based practices, where pruning is determined by model behavior on held out data.** FitPrune (Ye et al., 2025) adjusts selection by comparing attention distributions before and after pruning. VTW (Lin et al., 2025) locates layers after which token removal is reliably safe using calibration signals. **(3) A complementary perspective focuses on representativeness and semantic relevance.** TrimTokenator (Zhang et al., 2025a) estimates cross modal alignment with visual text mutual information and incorporates visual diversity for adaptive pruning. DivPrune (Alvar et al., 2025) retains a diverse subset by maximizing minimum pairwise token distance. ToDRE (Li et al., 2025a) handles diversity and task relevance as independent factors, selecting representative tokens and later filtering task irrelevant ones during decoding. CDPruner (Zhang et al., 2025b) formulates the task as conditional diversity maximization and applies a determinantal point process to obtain tokens.

3 Preliminaries and Challenges

3.1 Background of TrimTokenator

TrimTokenator (Zhang et al., 2025a) introduces two mutually reinforcing mechanisms that address visual token redundancy by jointly improving cross-modal alignment and greedily maximizing intra-modal representational coverage.

To ensure cross-modal semantic consistency, TrimTokenator estimates the value of each visual token by measuring its alignment with text tokens. Given the visual token set $\mathcal{X}^v = \{x_1^v, \dots, x_N^v\}$ and the text token set $\mathcal{X}^t = \{x_1^t, \dots, x_M^t\}$, the alignment score a_i for each visual token x_i^v is defined

as follows:

$$a_i = -\frac{1}{M} \sum_{j=1}^M \|x_i^v - x_j^t\|_2^2 \quad (1)$$

where smaller a_i values indicate that the visual token x_i^v is poorly aligned with textual semantics and should therefore be pruned. This scoring function facilitates the removal of semantically irrelevant regions, reducing visual noise and enhancing downstream text generation.

To enhance intra-modal representational diversity and reduce redundancy, TrimTokenator introduces a selection function $\text{GreedyRepMax}(\cdot)$. Given a visual token set \mathcal{X}^v and a target budget N , the function produces a subset $\hat{\mathcal{X}}_N^v$ by greedily choosing tokens that maximize dispersion in the embedding space, thereby covering broader and more complementary visual semantics. This procedure approximates the following objective:

$$\hat{\mathcal{X}}_N^v = \arg \max_{\mathcal{X} \subseteq \mathcal{X}^v, |\mathcal{X}|=N} \mathbb{E}_{x_i, x_j \in \mathcal{X}} D(x_i, x_j) \quad (2)$$

where $D(x_i, x_j)$ denotes the pairwise token distance between x_i and x_j . Guided by this objective, the selection can be expressed as follows:

$$\hat{\mathcal{X}}_N^v = \text{GreedyRepMax}(\mathcal{X}^v, N) \quad (3)$$

which yields a more dispersed and less redundant token subset that better covers visual semantics.

3.2 Key Challenges

In long context multi-image scenarios, the model needs to encode visual tokens drawn from multiple images simultaneously. There are four key challenges: **(1) Intra-Image and Inter-Image Redundancy Modeling** Multi-image inputs exhibit two forms of redundancy. Intra-image redundancy arises from repeated textures or similar local structures within a single image, while inter-image redundancy emerges when different images share similar subjects or layouts. Characterizing these two types of redundancy remains a challenging problem. **(2) Cross-Image Pruning Budget Allocation** Images vary widely in visual complexity and semantic contribution. A fixed pruning ratio often leaves simple images with an excess of redundant tokens while compressing complex images too aggressively. Consequently, dynamically allocating token budgets based on image content becomes essential for preserving critical information. **(3)**

Sequence of Intra-Image and Inter-Image Pruning Determining the order of these two stages is a key design decision. In this work, we prioritize intra-image pruning to first construct compact semantic bases for each image, ensuring that each image retains an independent and minimally sufficient representation. Placing inter-image pruning at the beginning would force all tokens to compete for a limited budget without constraints, which may result in some images being nearly pruned out, destroying their standalone semantic structure and causing their information to vanish from the overall representation. **(4) Position of Text Guided Alignment** Deciding whether to perform text guided alignment during the intra-image or inter-image pruning stage is an important consideration. Text alignment primarily targets global semantics rather than the local structure of individual images. Performing this during the inter-image pruning stage is more consistent with semantic reasoning, since textual descriptions typically capture relationships, key objects and trends across multiple images. The effectiveness of these design choices is verified in ablation studies.

4 Methodology

4.1 Overview

Given an image sequence (I_1, \dots, I_n) , the visual encoder produces for each image I_k a set of tokens $X_k = \{x_{k,1}, \dots, x_{k,m_k}\}$, where $m_k = |X_k|$ is the number of visual tokens for I_k . All tokens across the sequence can be represented as $X = \bigcup_{k=1}^n X_k$, with total size M_0 . We aim to retain only M_{final} tokens ($M_{final} < M_0$) such that the visual input remains both compact and comprehensive, while reducing computational cost. To achieve this, we perform intra-image pruning to compress the original token set X of each image, obtaining $X^{(1)}$ and reducing the total number of tokens from M_0 to M_1 . Then, we apply inter-image pruning to refine $X^{(1)}$ by removing cross-image redundancies, ultimately producing the final token set $X^{(*)}$ with M_{final} tokens. Figures 1 and 2 provide detailed and brief descriptions of our method, respectively.

Visual token redundancy in multi-image inputs arises from two structural sources. **(1) Intra-image redundancy** occurs when different regions within an image are semantically similar or structurally repetitive, generating many similar local tokens. **(2) Inter-image redundancy** arises when multiple images share repeated objects, scenes, or layouts.

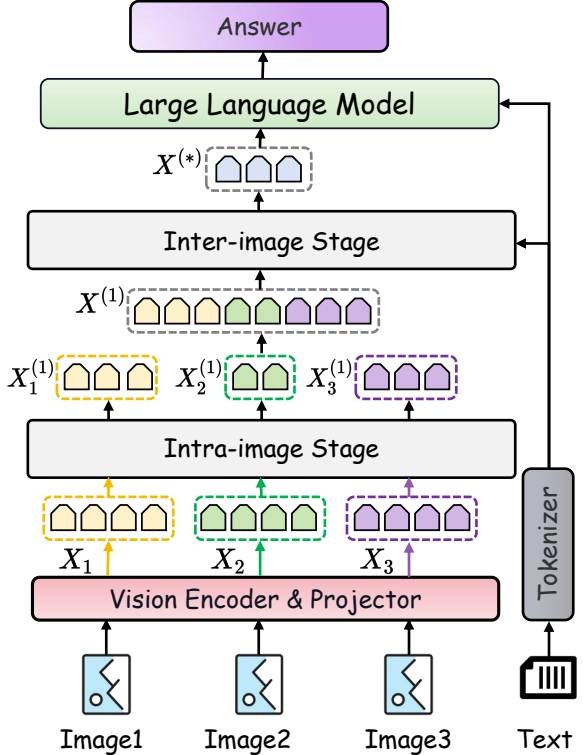


Figure 2: Brief overview of the visual token pruning method. Figure 1 provides a detailed description.

To adaptively control token retention, we introduce two metrics: **intra-image diversity** (\mathcal{D}_{intra}) and **inter-image variation** (\mathcal{D}_{inter}), capturing both the internal complexity of a single image and the differences across images. We provide a detailed analysis of the metrics in Appendix C.

\mathcal{D}_{intra} We define the intra-image diversity of an image I_k , denoted as $\mathcal{D}_{intra}(I_k)$, to measure the dispersion of visual tokens within the image, which is computed as follows:

$$\mathcal{D}_{intra}(I_k) = \frac{1}{m_k(m_k - 1)} \sum_{i \neq j} (1 - \cos(x_{k,i}, x_{k,j})) \quad (4)$$

Images with repetitive structures produce similar token representations, leading to lower $\mathcal{D}_{intra}(I_k)$, while images with richer content yield higher values. We further average this metric over all images to capture the overall intra-image complexity of the input set, which can be represented as follows:

$$\mathcal{D}_{intra} = \frac{1}{n} \sum_{k=1}^n \mathcal{D}_{intra}(I_k) \quad (5)$$

Higher \mathcal{D}_{intra} indicates richer internal visual content, suggesting that a higher token retention ratio should be used during intra-image pruning to preserve semantic structures.

\mathcal{D}_{inter} To capture semantic changes across images, we measure each image relative to its predecessor using global semantic embeddings. Specifically, we aggregate all visual tokens of I_k and I_{k-1} into their respective global representations and compute the cosine distance between them, defined as follows:

$$d_k = 1 - \cos\left(\frac{1}{m_k} \sum_{i=1}^{m_k} x_{k,i}, \frac{1}{m_{k-1}} \sum_{j=1}^{m_{k-1}} x_{k-1,j}\right) \quad (6)$$

where d_k approaches zero when consecutive images are nearly identical. Further details on why this metric is designed this way, rather than using a position-wise measure, can be found in Appendix C. To quantify the variation over the entire sequence, we average d_k across all consecutive image pairs to obtain the inter-image variation metric, which is defined as follows:

$$\mathcal{D}_{inter} = \frac{1}{n-1} \sum_{k=2}^n d_k \quad (7)$$

A higher \mathcal{D}_{inter} indicates greater differences between images, suggesting a higher token retention ratio during inter-image pruning to preserve semantic content across images.

To determine how many visual tokens should be preserved at the intra-image and inter-image pruning stages, we estimate the relative amount of redundancy within and across images. Using the intra-image diversity \mathcal{D}_{intra} and inter-image variation \mathcal{D}_{inter} , we introduce a factor s that captures both within-image complexity and cross-image differences, which can be represented as follows:

$$s = \frac{\mathcal{D}_{intra}}{\mathcal{D}_{inter}} \quad (8)$$

This factor provides an intuitive signal that when intra-image differences are large and cross-image variation is small, s becomes larger, resulting in a higher retention ratio at the intra-image pruning stage. Conversely, when cross-image variation dominates, s decreases, indicating that fewer tokens should be kept within each image so that more capacity can be allocated to modeling global semantic changes across images. We map this factor to an actual retention size using a transformation. Given the minimum and maximum intra-image budgets, M_{min} and M_{max} , and a scaling coefficient λ controlling the influence of s , we can define the target retention size M_1 for the intra-image pruning stage as follows:

$$M_1 = M_{min} + \lfloor (M_{max} - M_{min}) \cdot \lambda \cdot s \rfloor \quad (9)$$

Notably, we clip $\lambda \cdot s$ to the range $[0, 1]$. More details on the distribution of the s values can be found in Appendix H. This design allows adaptive retention. Experiments show our method performs well across various datasets and parameter settings, demonstrating strong generalization.

4.2 Intra-Image Processing Stage

The intra-image pruning stage aims to remove redundant tokens within each image, retaining tokens that best capture the core visual structure. We assign a retention weight to each image based on its intra-image diversity. For image I_k , the weight w_k is defined as follows:

$$w_k = \mathcal{D}_{intra}(I_k) \quad (10)$$

where a higher weight indicates that the image requires more tokens to be retained. The last image in a sequence often carries more importance for the response and receives higher attention. Thus, when there are more than two images (for two images, which often correspond to each other, their relative importance is typically comparable), the retention weight of the last image is set as follows:

$$w_n = \max_k w_k \quad \text{if } n > 2 \quad (11)$$

Given these weights, the number of tokens $m_k^{(1)}$ to retain for image I_k during intra-image pruning is computed as follows:

$$m_k^{(1)} = \lfloor \frac{w_k}{\sum_{j=1}^n w_j} \cdot M_1 \rfloor \quad (12)$$

With the retention count determined for each image, we apply *GreedyRepMax* (Equation 3) to select the $m_k^{(1)}$ most representative tokens $X_k^{(1)}$ from the original token set X_k , as follows:

$$X_k^{(1)} = \text{GreedyRepMax}(X_k, m_k^{(1)}) \quad (13)$$

The output $X^{(1)}$ of this stage can be expressed as follows:

$$X^{(1)} = \bigcup_{k=1}^n X_k^{(1)}, \quad |X^{(1)}| = M_1 \quad (14)$$

4.3 Inter-Image Processing Stage

The inter-image pruning stage aims to extract the most critical semantic information across all images, obtaining the final set $X^{(*)}$ of M_{final} tokens. We first apply a global *GreedyRepMax* on $X^{(1)}$

to maximize the coverage of token representations and retain M_2 tokens, with result $X^{(2)}$ as follows:

$$X^{(2)} = \text{GreedyRepMax}(X^{(1)}, M_2) \quad (15)$$

Next, to further select tokens that contribute most across images and are well-aligned with the text, we use two metrics for each token x_i , namely inter-image diversity v_i and text alignment a_i . These metrics are defined as follows:

$$v_i = \frac{1}{|X^{(2)}| - 1} \sum_{j \neq i} (1 - \cos(x_i, x_j)) \quad (16)$$

$$a_i = -\frac{1}{|X^t|} \sum_{t \in X^t} \|x_i - t\|_2^2 \quad (17)$$

Here, X^t is the textual token set. We use *Pareto* selection to choose the set of tokens from $X^{(2)}$ that are optimal in both metrics. More details on *Pareto* selection can be found in Appendix B. The result $X^{(*)}$ can be represented as follows:

$$X^{(*)} = \text{Pareto}(X^{(2)}, \{v_i\}, \{a_i\}, M_{final}) \quad (18)$$

where $\{v_i\}$ and $\{a_i\}$ represent the inter-image diversity and text alignment scores of all tokens in $X^{(2)}$, respectively. The resulting set $X^{(*)}$, containing M_{final} tokens, is subsequently fed into the language model.

5 Experiments

5.1 Experimental Setup

Models and Baselines. To evaluate the effectiveness of our method, we perform extensive experiments on a diverse set of representative LMMs, including LLaVA-1.5-7B (Liu et al., 2023), LLaVA-1.5-13B (Liu et al., 2023), Yi-VL-6B (Young et al., 2024) and InternVL-Chat-ViT-6B-Vicuna-13B (Chen et al., 2024b). These models span a wide range of parameter scales and architectures. We compare our method against a set of widely used pruning baselines, including FastV (Chen et al., 2024a), VTW (Lin et al., 2025), SparseVLM (Zhang et al., 2024b), VisionZip (Yang et al., 2025), CATP (Li et al., 2025c), DivPrune (Alvar et al., 2025) and TrimTokenator (Zhang et al., 2025a). All baselines are assessed under consistent experimental settings to ensure a rigorous and fair comparison.

Datasets and Metrics. We evaluate our method on a series of benchmark datasets, including ActionPrediction (ActPred) (Wu et al., 2024), ALFRED (Shridhar et al., 2020), CounterfactualInference (CFInfer) (Yi et al., 2019), IEdit (Tan

et al., 2019), MovingDirection (MoveDir) (Yi et al., 2019), MultiModalQA (MMQA) (Talmor et al., 2021), ObjectExistence (ObjExist) (Yi et al., 2019), ObjectShuffle (ObjShuf) (Patraucean et al., 2023) and OCR-VQA (Mishra et al., 2019). These datasets include from just a few to over a hundred images and cover diverse tasks, offering a comprehensive evaluation setting. We employ accuracy to evaluate performance on understanding datasets, and Rouge-L for generative datasets.

Implementation Details. We utilize an NVIDIA H100 GPU with 80GB of memory. We set the default values of the parameters M_{min} , M_{max} , λ and M_2 to 294, 454, 0.5 and 252, respectively. We set the default token retention ratio to 0.2 in both the comparative and ablation experiments. More details can be found in Appendix H.

5.2 Main Results

Table 1 reports the comparative performance of our method across multiple LMMs under a token retention ratio of 0.2. We evaluate it against the original model as well as a range of token pruning methods. The results demonstrate that our method consistently outperforms competing approaches across different model scales and tasks, highlighting its effectiveness in long context multimodal scenarios. On LLaVA-1.5-7B, our method consistently surpasses strong baselines such as FastV, VTW and DivPrune. Specifically, for the ActionPrediction task, our method achieves a performance of 56.0, showing a clear improvement over FastV and TrimTokenator. Moreover, in some cases, performance even exceeds the original model, likely due to denser critical information and less irrelevant visual noise. Our approach exhibits remarkable robustness: on LLaVA-1.5-13B, it outperforms the original model across tasks such as ObjectShuffle and OCR-VQA. Furthermore, our method demonstrates strong generalization capabilities, achieving excellent performance on the Yi-VL-6B architecture as well. At the same token retention ratio, it consistently surpasses other baselines across a wide range of tasks. These findings validate the robustness of our method across different model architectures and its scalability to models of various sizes. Additionally, we provide the performance comparison of InternVL-Chat-ViT-6B-Vicuna-13B in Appendix D. We also provide the performance comparison of various methods under a different token retention ratio in Appendix E.

Method	ActPred	ALFRED	CFInfer	IEdit	MoveDir	MMQA	ObjExist	ObjShuf	OCR-VQA
LLaVA-1.5-7B									
Original Model	52.0	14.81	30.5	5.36	32.0	67.0	50.5	34.5	8.0
FastV	52.5	9.82	22.5	4.26	18.0	61.0	40.5	32.0	3.5
VTW	52.0	10.28	22.0	4.37	19.5	60.5	42.0	31.5	2.5
SparseVLM	53.5	11.06	23.0	5.03	20.5	62.0	44.5	33.0	3.0
VisionZip	53.5	11.18	22.5	4.43	22.5	61.0	42.5	32.5	3.0
CATP	51.5	10.32	21.0	4.21	17.0	60.5	39.0	31.5	3.5
DivPrune	54.0	11.31	22.5	4.61	17.5	62.0	36.0	32.5	3.0
TrimTokenator	54.0	11.26	23.5	4.52	22.0	61.5	43.0	33.0	3.5
Ours	56.0	12.74	25.0	5.15	25.5	62.5	47.0	33.5	4.5
LLaVA-1.5-13B									
Original Model	45.0	18.64	38.0	9.00	37.0	70.5	47.0	40.5	46.0
FastV	46.0	15.17	34.0	7.48	32.5	66.5	46.0	40.5	45.5
VTW	46.5	15.35	34.5	7.61	33.5	66.0	45.5	39.5	46.0
SparseVLM	47.0	16.21	37.0	7.96	33.5	67.0	48.0	41.0	47.5
VisionZip	46.5	15.76	36.5	7.82	32.5	67.5	47.5	39.5	47.0
CATP	44.5	15.62	34.0	7.57	32.0	66.5	45.5	40.0	45.5
DivPrune	47.5	15.50	37.0	8.30	34.0	66.0	47.5	40.5	46.5
TrimTokenator	47.0	16.25	36.5	8.15	33.5	67.0	47.0	39.5	47.0
Ours	48.5	18.14	38.0	8.35	35.5	69.0	51.5	42.5	49.5
Yi-VL-6B									
Original Model	40.5	16.02	36.5	7.90	21.0	67.0	53.0	36.5	27.5
FastV	39.0	17.62	31.0	7.12	28.5	63.0	50.5	30.5	23.0
VTW	40.0	17.87	31.5	7.25	27.0	65.5	51.0	30.0	23.5
SparseVLM	39.5	18.35	32.0	7.18	29.0	64.0	52.0	30.5	24.5
VisionZip	40.5	18.17	32.5	7.29	28.0	63.0	53.5	31.0	24.0
CATP	39.5	17.82	31.5	7.15	28.5	63.5	51.5	29.5	23.5
DivPrune	40.0	18.76	33.0	7.45	29.5	66.0	55.0	31.5	25.0
TrimTokenator	39.5	18.67	32.5	7.40	29.0	64.5	53.5	30.5	24.0
Ours	40.5	19.84	34.0	7.59	30.0	67.5	55.5	32.5	25.5

Table 1: Performance comparison of different methods across multiple models and tasks at a retention ratio of 0.2.

5.3 Efficiency Analysis (Accounting for Pruning Overhead)

We conduct efficiency tests on LLaVA-1.5-7B in FP16 precision using images with lengths ranging from 2 to 32, with inputs also in FP16, and a batch size of 1. Specifically, under the same pruning ratio as in the main experiments, we measure inference latency and GPU memory usage. It is important to emphasize that the reported latency corresponds to the prefill stage, as the pruning operations are performed during this stage. By the time the decoding stage begins, all pruning is already complete; therefore, the measured latency fully accounts for the overhead introduced by the pruning process. As

presented in Table 2, our method achieves acceleration in inference and a notable reduction in memory consumption, offering a practical and effective solution for deploying long context multimodal models in resource-constrained environments. More details on pruning acceleration can be found in Appendix J.

5.4 Ablation Study

To comprehensively analyze the contribution of each component in our method, we conduct extensive ablation studies on LLaVA-1.5-7B, with the results summarized in Table 3. We first examine the necessity of the two stage architecture and its sequential design. Specifically, we consider three

Method	Original	FastV	VTW	SparseVLM	VisionZip	CATP	DivPrune	Ours
Latency (ms)	1035.47	825.91	813.85	821.01	813.05	827.92	810.46	802.65
Memory (G)	19.38	15.34	15.27	15.33	15.20	15.37	15.20	15.18

Table 2: Comparison of GPU memory and latency for our pruning method and baselines on LLaVA-1.5-7B.

ablation settings: *Ablation*₁, which completely removes the intra-image pruning stage; *Ablation*₂, which removes the inter-image pruning stage; and *Ablation*₃, which swaps the execution order by performing inter-image pruning before intra-image. As shown in the results, all three variants lead to consistent performance degradation. These findings indicate that eliminating local redundancy is a prerequisite for effective global modeling, and that modeling cross-image variations is crucial for long context understanding. Moreover, token pruning must first be conducted at the single image level to obtain compact image representations, upon which accurate global pruning of cross-image redundancy can be performed. We further investigate the impact of the dynamic budget allocation and the text alignment pareto selection strategy. In *Ablation*₄, we remove dynamic budget allocation and instead assign a fixed and uniform budget to each image. In *Ablation*₅, we disable the pareto selection mechanism entirely. In *Ablation*₆, pareto selection is prematurely applied during the intra-image pruning stage while being omitted in the inter-image stage. All these ablations result in performance drops, demonstrating the importance of dynamic budget allocation as well as applying pareto selection at the inter-image level. More ablation results can be found in Appendix F.

Setting	ActPred	CFInfer	MoveDir	ObjExist	OCR-VQA
<i>Ablation</i> ₁	55.0	24.0	24.5	45.0	2.5
<i>Ablation</i> ₂	54.0	24.0	25.0	45.5	4.0
<i>Ablation</i> ₃	53.0	22.0	23.0	45.5	2.5
<i>Ablation</i> ₄	54.5	23.5	23.0	45.5	4.0
<i>Ablation</i> ₅	53.0	22.0	18.5	41.0	2.5
<i>Ablation</i> ₆	55.0	22.5	19.0	41.0	4.0
Ours	56.0	25.0	25.5	47.0	4.5

Table 3: Performance comparison under different ablation settings on LLaVA-1.5-7B across benchmarks.

5.5 Performance on Different Retention Ratios

We analyze the performance trends of LLaVA-1.5-7B on the representative tasks ALFRED and CFInfer under different visual token retention ratios, ranging from 0.1 to 0.5. As shown in Figure 3,

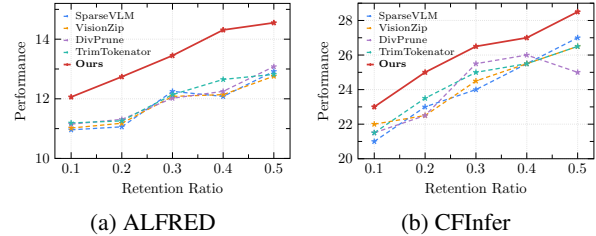


Figure 3: Performance across different token retention ratios with LLaVA-1.5-7B.

our method consistently and significantly outperforms all baseline methods across all retention settings. Specifically, even under the most stringent retention ratio of 0.1, our method achieves a performance of 12.06 on ALFRED, substantially surpassing the others. This notable gap indicates that our approach effectively preserves crucial information, whereas strategies that rely solely on local information tend to struggle with this task. Furthermore, as the retention ratio increases to 0.5, our performance advantage is not only maintained but further widened, clearly exceeding other methods and demonstrating the robustness of our approach.

6 Conclusion

In this paper, we explore the challenges of visual token pruning in long context multi-image inputs. Based on this, we propose an adaptive pruning method that uses intra-image diversity and inter-image variation to model the two types of redundancy. Our method consists of two stages: intra-image pruning and inter-image pruning. The intra-image pruning allocates token budgets adaptively based on each image’s visual richness and uses a greedy strategy to select the most representative tokens for each image. The inter-image pruning performs global diversity filtering over all image tokens to form a candidate set and then applies Pareto selection based on diversity and text alignment to retain the most informative and text-relevant tokens. Extensive experiments demonstrate the soundness and effectiveness of our method.

Limitations

In this work, we conduct experiments across multiple models and datasets to evaluate the effectiveness of our proposed multimodal long context visual token pruning method. The results demonstrate the validity of our approach. However, due to computational constraints, we have not yet evaluated it on extremely large models, such as those with 70 billion parameters. Exploring the scalability of our method to such large models constitutes an important direction for future work.

References

Saeed Ranjbar Alvar, Gursimran Singh, Mohammad Akbari, and Yong Zhang. 2025. Divprune: Diversity-based visual token pruning for large multimodal models. *arXiv preprint arXiv:2503.02175*.

Shuai Bai, Keqin Chen, Xuejing Liu, Jialin Wang, Wenbin Ge, Sibo Song, Kai Dang, Peng Wang, Shijie Wang, Jun Tang, and 1 others. 2025. Qwen2. 5-vl technical report. *arXiv preprint arXiv:2502.13923*.

T Brown, B Mann, N Ryder, M Subbiah, JD Kaplan, P Dhariwal, A Neelakantan, P Shyam, G Sastry, A Askell, and 1 others. 2020. Language models are few-shot learners advances in neural information processing systems 33.

Mu Cai, Jianwei Yang, Jianfeng Gao, and Yong Jae Lee. 2024. Matryoshka multimodal models. In *Workshop on Video-Language Models@ NeurIPS 2024*.

Kevin Chen, Jiayuan Li, Yang Li, and Zhen Li. 2023. [A survey on efficient transformer models](#). *arXiv preprint*.

Liang Chen, Haozhe Zhao, Tianyu Liu, Shuai Bai, Junyang Lin, Chang Zhou, and Baobao Chang. 2024a. An image is worth 1/2 tokens after layer 2: Plug-and-play inference acceleration for large vision-language models. In *European Conference on Computer Vision*, pages 19–35. Springer.

Zhe Chen, Weiyun Wang, Yue Cao, Yangzhou Liu, Zhangwei Gao, Erfei Cui, Jinguo Zhu, Shenglong Ye, Hao Tian, Zhaoyang Liu, and 1 others. 2024b. Expanding performance boundaries of open-source multimodal models with model, data, and test-time scaling. *arXiv preprint arXiv:2412.05271*.

Wei-Lin Chiang, Zhuohan Li, Ziqing Lin, Ying Sheng, Zhanghao Wu, Hao Zhang, Lianmin Zheng, Siyuan Zhuang, Yonghao Zhuang, Joseph E Gonzalez, and 1 others. 2023. Vicuna: An open-source chatbot impressing gpt-4 with 90%* chatgpt quality. *See https://vicuna.lmsys.org (accessed 14 April 2023)*, 2(3):6.

Hugging Face. 2024. *Mastering Transformers: The Journey from BERT to Large Language Models and Stable Diffusion*. Open Library.

E. Huang and 1 others. 2023. Evaluating large language models in complex scenarios. *Journal of Computational Linguistics*.

Kai Huang, Hao Zou, Ye Xi, BoChen Wang, Zhen Xie, and Liang Yu. 2024. Ivtp: Instruction-guided visual token pruning for large vision-language models. In *European Conference on Computer Vision*, pages 214–230. Springer.

Feyza Duman Keles, Pruthuvi Mahesakya Wijewardena, and Chinmay Hegde. 2023. On the computational complexity of self-attention. In *International conference on algorithmic learning theory*, pages 597–619. PMLR.

C. Li and 1 others. 2023. Fine-tuning techniques for efficient model adaptation. *AI Research Journal*.

Duo Li, Zuhao Yang, and Shijian Lu. 2025a. Todre: Visual token pruning via diversity and task awareness for efficient large vision-language models. *arXiv preprint arXiv:2505.18757*.

Wentong Li, Yuqian Yuan, Jian Liu, Dongqi Tang, Song Wang, Jie Qin, Jianke Zhu, and Lei Zhang. 2025b. Tokenpacker: Efficient visual projector for multimodal llm. *International Journal of Computer Vision*, pages 1–19.

Yanshu Li, Jianjiang Yang, Zhennan Shen, Ligong Han, Haoyan Xu, and Ruixiang Tang. 2025c. Catp: Contextually adaptive token pruning for efficient and enhanced multimodal in-context learning. *arXiv preprint arXiv:2508.07871*.

Bin Lin, Yang Ye, Bin Zhu, Jiaxi Cui, Munan Ning, Peng Jin, and Li Yuan. 2023. Video-llava: Learning united visual representation by alignment before projection. *arXiv preprint arXiv:2311.10122*.

Zhihang Lin, Mingbao Lin, Luxi Lin, and Rongrong Ji. 2025. Boosting multimodal large language models with visual tokens withdrawal for rapid inference. In *Proceedings of the AAAI Conference on Artificial Intelligence*, volume 39, pages 5334–5342.

Haotian Liu, Chunyuan Li, Yuheng Li, and Yong Jae Lee. 2024a. Improved baselines with visual instruction tuning. In *Proceedings of the IEEE/CVF Conference on Computer Vision and Pattern Recognition*, pages 26296–26306.

Haotian Liu, Chunyuan Li, Qingyang Wu, and Yong Jae Lee. 2023. Visual instruction tuning. *Advances in neural information processing systems*, 36:34892–34916.

Shizhan Liu, Hang Yu, Cong Liao, Jianguo Li, Weiyao Lin, Alex X Liu, and Schahram Dustdar. 2022. Pyraformer: Low-complexity pyramidal attention for long-range time series modeling and forecasting. In *# PLACEHOLDER_PARENT_METADATA_VALUE#*.

Ting Liu, Liangtao Shi, Richang Hong, Yue Hu, Quanjun Yin, and Linfeng Zhang. 2024b. Multi-stage vision token dropping: Towards efficient multimodal large language model. *arXiv preprint arXiv:2411.10803*.

Anand Mishra, Shashank Shekhar, Ajeet Kumar Singh, and Anirban Chakraborty. 2019. Ocr-vqa: Visual question answering by reading text in images. In *2019 international conference on document analysis and recognition (ICDAR)*, pages 947–952. IEEE.

Adam Paszke, Sam Gross, Francisco Massa, Adam Lerer, James Bradbury, Gregory Chanan, Trevor Killeen, Zeming Lin, Natalia Gimelshein, Luca Antiga, and 1 others. 2019. Pytorch: An imperative style, high-performance deep learning library. *Advances in neural information processing systems*, 32.

Viorica Patraucean, Lucas Smaira, Ankush Gupta, Adria Recasens, Larisa Markeeva, Dylan Banarse, Skanda Koppula, Mateusz Malinowski, Yi Yang, Carl Doersch, and 1 others. 2023. Perception test: A diagnostic benchmark for multimodal video models. *Advances in Neural Information Processing Systems*, 36:42748–42761.

Yuzhang Shang, Mu Cai, Bingxin Xu, Yong Jae Lee, and Yan Yan. 2024. Llava-prumerge: Adaptive token reduction for efficient large multimodal models. *arXiv preprint arXiv:2403.15388*.

Mohit Shridhar, Jesse Thomason, Daniel Gordon, Yonatan Bisk, Winson Han, Roozbeh Mottaghi, Luke Zettlemoyer, and Dieter Fox. 2020. Alfred: A benchmark for interpreting grounded instructions for everyday tasks. In *Proceedings of the IEEE/CVF conference on computer vision and pattern recognition*, pages 10740–10749.

Yizheng Sun, Yanze Xin, Hao Li, Chenghua Lin, and Riza Batista-Navarro. 2023. Velar: Vision-oriented language-attentive token reduction for multimodal large language models.

Yizheng Sun, Yanze Xin, Hao Li, Jingyuan Sun, Chenghua Lin, and Riza Batista-Navarro. 2025. Lvpruning: An effective yet simple language-guided vision token pruning approach for multi-modal large language models. *arXiv preprint arXiv:2501.13652*.

Alon Talmor, Ori Yoran, Amnon Catav, Dan Lahav, Yizhong Wang, Akari Asai, Gabriel Ilharco, Hanneh Hajishirzi, and Jonathan Berant. 2021. Multimodalqa: Complex question answering over text, tables and images. *arXiv preprint arXiv:2104.06039*.

Hao Tan, Franck Dernoncourt, Zhe Lin, Trung Bui, and Mohit Bansal. 2019. Expressing visual relationships via language. *arXiv preprint arXiv:1906.07689*.

Kimi Team, Angang Du, Bohong Yin, Bowei Xing, Bowen Qu, Bowen Wang, Cheng Chen, Chenlin Zhang, Chenzhuang Du, Chu Wei, and 1 others. 2025. Kimi-vl technical report. *arXiv preprint arXiv:2504.07491*.

Jintao Tong, Wenwei Jin, Pengda Qin, Anqi Li, Yixiong Zou, Yuhong Li, Yuhua Li, and Ruixuan Li. 2025. Flowcut: Rethinking redundancy via information flow for efficient vision-language models. *arXiv preprint arXiv:2505.19536*.

H Touvron, T Lavril, G Izacard, X Martinet, MA Lachaux, T Lacroix, B Rozière, N Goyal, E Hambré, F Azhar, and 1 others. 2023. Open and efficient foundation language models. *Preprint at arXiv*. <https://doi.org/10.48550/arXiv.2302>.

Ashish Vaswani, Noam Shazeer, Niki Parmar, Jakob Uszkoreit, Llion Jones, Aidan N Gomez, Łukasz Kaiser, and Illia Polosukhin. 2017. *Attention is all you need*. *arXiv preprint*.

F. Wang and 1 others. 2023. Practical applications of llms in specialized domains. *Specialized AI Applications*.

Thomas Wolf. 2020. Transformers: State-of-the-art natural language processing. *arXiv preprint arXiv:1910.03771*.

Bo Wu, Shoubin Yu, Zhenfang Chen, Joshua B Tenenbaum, and Chuang Gan. 2024. Star: A benchmark for situated reasoning in real-world videos. *arXiv preprint arXiv:2405.09711*.

Senqiao Yang, Yukang Chen, Zhuotao Tian, Chengyao Wang, Jingyao Li, Bei Yu, and Jiaya Jia. 2025. Visionzip: Longer is better but not necessary in vision language models. In *Proceedings of the Computer Vision and Pattern Recognition Conference*, pages 19792–19802.

Weihao Ye, Qiong Wu, Wenhao Lin, and Yiyi Zhou. 2025. Fit and prune: Fast and training-free visual token pruning for multi-modal large language models. In *Proceedings of the AAAI Conference on Artificial Intelligence*, pages 22128–22136.

Kexin Yi, Chuang Gan, Yunzhu Li, Pushmeet Kohli, Jiajun Wu, Antonio Torralba, and Joshua B Tenenbaum. 2019. Clevrer: Collision events for video representation and reasoning. *arXiv preprint arXiv:1910.01442*.

Alex Young, Bei Chen, Chao Li, Chengan Huang, Ge Zhang, Guanwei Zhang, Guoyin Wang, Heng Li, Jiangcheng Zhu, Jianqun Chen, and 1 others. 2024. Yi: Open foundation models by 01. ai. *arXiv preprint arXiv:2403.04652*.

D. Zhang and 1 others. 2023. Parameter-efficient fine-tuning methods for llms. *Journal of Machine Learning Research*.

Hao Zhang, Mengsi Lyu, Chenrui He, Yulong Ao, and Yonghua Lin. 2025a. Trimitokenator: Towards adaptive visual token pruning for large multimodal models. *arXiv preprint arXiv:2509.00320*.

Qizhe Zhang, Aosong Cheng, Ming Lu, Zhiyong Zhuo, Minqi Wang, Jiajun Cao, Shaobo Guo, Qi She, and Shanghang Zhang. 2024a. [cls] attention is all you need for training-free visual token pruning: Make vlm inference faster. *arXiv preprint arXiv:2412.01818*.

Qizhe Zhang, Mengzhen Liu, Lichen Li, Ming Lu, Yuan Zhang, Junwen Pan, Qi She, and Shanghang Zhang. 2025b. Beyond attention or similarity: Maximizing conditional diversity for token pruning in mllms. *arXiv preprint arXiv:2506.10967*.

Yuan Zhang, Chun-Kai Fan, Junpeng Ma, Wenzhao Zheng, Tao Huang, Kuan Cheng, Denis Gudovskiy, Tomoyuki Okuno, Yohei Nakata, Kurt Keutzer, and 1 others. 2024b. Sparsevlm: Visual token sparsification for efficient vision-language model inference. *arXiv preprint arXiv:2410.04417*.

B. Zhu and 1 others. 2023. Expanding frontiers in large language models. *AI Frontier Research*.

Jinguo Zhu, Weiyun Wang, Zhe Chen, Zhaoyang Liu, Shenglong Ye, Lixin Gu, Yuchen Duan, Hao Tian, Weijie Su, Jie Shao, and 1 others. 2025. Internvl3: Exploring advanced training and test-time recipes for open-source multimodal models. *arXiv preprint arXiv:2504.10479*.

A Algorithm Overview

We outline the overall procedure of TrimTokenator-LC in Algorithm 1, which provides the pseudocode of our proposed method.

B Details of Pareto Selection

Pareto selection is a multi-objective optimization method used to select an optimal set of solutions when multiple conflicting objectives exist. Its core idea is based on the concept of a non-dominated

solution. A solution is considered non-dominated if no other solution is better in all objectives simultaneously. All non-dominated solutions form the Pareto front, representing the trade-off between different objectives. Formally, given two objective functions $f_1(x)$ and $f_2(x)$, a candidate solution x_i is Pareto optimal if there does not exist another solution x_j such that $f_1(x_j) \geq f_1(x_i)$ and $f_2(x_j) \geq f_2(x_i)$, with at least one strict inequality, that is, $(f_1(x_j) > f_1(x_i))$ or $(f_2(x_j) > f_2(x_i))$. More details on how this problem is addressed can be found in Appendix J.

Algorithm 1 TrimTokenator-LC

Require: Visual token sets (X_1, \dots, X_n) , where $X_k = \{x_{k,1}, \dots, x_{k,m_k}\}$; text tokens X_t ; final budget M_{final} ; budgets M_{min} and M_{max} , scaling coefficient λ and candidate budget M_2
Ensure: Final visual token set $X^{(*)}$

```

1: /* Compute Redundancy Signals */
2: for  $k = 1$  to  $n$  do
3:   Compute Intra-Image Diversity  $\mathcal{D}_{intra}(I_k)$ 
4: end for
5:  $\mathcal{D}_{intra} \leftarrow \frac{1}{n} \sum_{k=1}^n \mathcal{D}_{intra}(I_k)$ 
6: for  $k = 2$  to  $n$  do
7:   Compute Inter-Image Variation  $d_k$ 
8: end for
9:  $\mathcal{D}_{inter} \leftarrow \frac{1}{n-1} \sum_{k=2}^n d_k$ 
10:  $s \leftarrow \mathcal{D}_{intra}/\mathcal{D}_{inter}$ 
11:  $M_1 \leftarrow M_{min} + \lfloor (M_{max} - M_{min}) \cdot \lambda \cdot s \rfloor$ 
12: /* Intra-Image Processing Stage */
13: for  $k = 1$  to  $n$  do
14:    $w_k \leftarrow \mathcal{D}_{intra}(I_k)$ 
15: end for
16: if  $n > 2$  then
17:    $w_n \leftarrow \max_k w_k$ 
18: end if
19: for  $k = 1$  to  $n$  do
20:    $m_k^{(1)} \leftarrow \lfloor \frac{w_k}{\sum_{j=1}^n w_j} \cdot M_1 \rfloor$ 
21:    $X_k^{(1)} \leftarrow GreedyRepMax(X_k, m_k^{(1)})$ 
22: end for
23:  $X^{(1)} \leftarrow \bigcup_{k=1}^n X_k^{(1)}$ 
24: /* Inter-Image Processing Stage */
25:  $X^{(2)} \leftarrow GreedyRepMax(X^{(1)}, M_2)$ 
26: for all  $x_i \in X^{(2)}$  do
27:    $v_i \leftarrow \frac{1}{|X^{(2)}|-1} \sum_{j \neq i} (1 - \cos(x_i, x_j))$ 
28:    $a_i \leftarrow -\frac{1}{|X^{(2)}|} \sum_{t \in X^{(2)}} \|x_i - t\|_2^2$ 
29: end for
30:  $X^{(*)} \leftarrow Pareto(X^{(2)}, \{v_i\}, \{a_i\}, M_{final})$ 
31: return  $X^{(*)}$ 

```

C Metric Analysis

Intra-image diversity is designed to quantify the degree of dispersion among visual tokens within a single image in the embedding space. This metric is motivated by the need for minimal semantic coverage per image in long context settings. During visual encoding, an image is typically mapped to a large number of local tokens, many of which originate from semantically or structurally similar regions whose marginal information contribution quickly diminishes. When an image is dominated by large homogeneous backgrounds or repetitive textures, token representations tend to be highly similar, resulting in low intra-image diversity and indicating substantial internal redundancy. In contrast, images containing multiple objects or complex spatial structures yield more dispersed token representations in the embedding space, leading to higher intra-image diversity. Defined as the average cosine distance among tokens within the same image, this metric directly reflects the number of independent visual prototypes present in the image. It therefore provides a quantitative criterion for determining whether more tokens should be preserved during pruning to maintain the image's fundamental semantic structure, effectively preventing excessive compression of visually complex images.

Inter-image variation is designed to characterize the degree of semantic change between images in long context inputs. Treating all image tokens as independent is unreasonable when the visual content is redundant. To address this issue, we quantify the amount of new information introduced by the current image I_k relative to its predecessor I_{k-1} by comparing their global semantic embeddings. Specifically, we aggregate all visual tokens of each image into a single global representation and compute the cosine distance between consecu-

Method	ActPred	ALFRED	CFInfer	IEdit	MoveDir	MMQA	ObjExist	ObjShuf	OCR-VQA
<i>Original Model</i>	51.0	16.20	30.0	10.74	29.0	66.0	50.5	37.0	16.5
<i>FastV</i>	48.0	13.73	28.5	9.82	33.0	58.0	45.5	36.0	10.5
<i>VTW</i>	49.0	13.62	27.5	9.75	32.5	59.5	46.0	36.5	11.5
<i>SparseVLM</i>	50.5	14.94	28.0	10.32	32.0	60.5	46.5	37.0	11.0
<i>VisionZip</i>	52.0	14.76	28.5	10.28	33.5	58.5	45.5	35.5	11.5
<i>CATP</i>	51.0	14.15	25.0	10.12	32.5	58.0	45.0	35.5	12.0
<i>DivPrune</i>	52.0	15.23	26.5	10.77	34.0	62.5	48.5	37.0	12.5
<i>TrimTokenator</i>	51.5	15.12	26.0	10.61	32.0	62.0	48.0	36.0	11.5
Ours	54.0	16.10	30.0	11.34	34.5	63.0	49.0	37.5	13.0

Table 4: Performance comparison of visual token pruning methods on InternVL-Chat-ViT-6B-Vicuna-13B.

tive images. When neighboring images are highly similar or repetitive, their global embeddings are strongly aligned, yielding a small inter-image variation value, which indicates that cross-image redundancy dominates. Because this metric captures global semantic transitions across images rather than local token fluctuations, it provides a stable and direct quantitative criterion for preserving the most critical visual information needed to model semantic evolution in long context scenarios. Furthermore, we consider methods that estimate inter-image changes based on position-wise differences of visual tokens, which can represent as follows:

$$d_k = \frac{1}{m_k} \sum_{i=1}^{m_k} (1 - \cos(x_{k,i}, x_{k-1,i})) \quad (19)$$

Such approaches implicitly assume that the spatial structure across different images is consistently aligned, i.e., tokens at the same index are semantically comparable. However, this assumption often does not hold in long context scenarios: images from different sources (e.g., webpages, slides or unrelated photos) generally lack strict spatial correspondence; even consecutive images from the same source may experience spatial shifts due to viewpoint changes, content rearrangement or significant object motion, making "corresponding tokens" no longer truly semantically aligned. Relying on position-wise matching in such cases can not only introduce noisy estimates but also systematically underestimate the true cross-image semantic changes. Moreover, in some tasks, consecutive images may be entirely different (e.g., two different documents or unrelated objects). Comparing the top-left region of a document with that of a natural image yields a ‘variation’ score driven by spatial misalignment rather than semantic redundancy.

D Performance Comparison on InternVL-Chat-ViT-6B-Vicuna-13B

To further validate the generality of our method, we extend our evaluation to the InternVL-Chat-ViT-6B-Vicuna-13B model, which employs a substantially larger visual encoder than the LLaVA family. As shown in Table 4, our method consistently outperforms the baselines on this architecture, achieving the best performance on various tasks. By selectively retaining visually informative tokens, our approach effectively reduces computational overhead while improving the quality of the preserved visual context. These results further demonstrate the strong robustness of our method and highlight its ability to generalize effectively across different model architectures.

E Performance Comparison under a Different Token Retention Ratio

We further evaluate the model performance on LLaVA-1.5-7B under a higher token retention ratio of 0.5. As shown in Table 5, our method continues to outperform all other pruning strategies, demonstrating that it maintains a clear advantage even under relatively high token retention settings. This result highlights the robustness of our approach, indicating that selectively preserving informative tokens can consistently enhance performance without being overly sensitive to the retention ratio.

F More Ablation Results

We conduct additional ablation studies to further analyze our design choices. Specifically, during the adaptive allocation of the image budget, we apply a special treatment to the last image (Eq. 11). We define a variant that removes this component as *Allocation*₁. In addition, we enforce an equal

Method	ActPred	ALFRED	CFInfer	IEdit	MoveDir	MMQA	ObjExist	ObjShuf	OCR-VQA
<i>Original Model</i>	52.0	14.81	30.5	5.36	32.0	67.0	50.5	34.5	8.0
<i>FastV</i>	46.0	11.68	25.5	6.85	25.0	63.0	46.5	16.0	6.0
<i>VTW</i>	47.5	11.92	25.0	7.03	25.5	64.5	46.0	15.5	7.0
<i>SparseVLM</i>	49.0	12.92	27.0	7.18	26.0	65.5	47.5	16.5	6.5
<i>VisionZip</i>	48.5	12.76	26.5	7.24	26.5	65.5	48.5	16.5	7.5
<i>CATP</i>	47.5	12.07	25.5	7.17	25.5	63.0	46.5	16.0	6.0
<i>DivPrune</i>	48.5	13.08	25.0	7.35	27.0	66.5	48.5	16.5	7.5
<i>TrimTokenator</i>	47.0	12.82	26.5	7.25	26.5	65.0	47.0	17.0	8.0
Ours	50.0	14.55	28.5	8.10	27.5	65.5	50.0	18.5	9.0

Table 5: Comparative results of different pruning methods on LLaVA-1.5-7B under a token retention ratio of 0.5.

number of pruned tokens for intra-image and inter-image pruning, with half of the tokens pruned at each stage. This allocation strategy is denoted as *Allocation*₂, and is used to evaluate the effectiveness of our two stage adaptive allocation scheme. As shown in Table 6, both allocation strategies lead to performance degradation to varying degrees. On OCR-VQA, our method performs comparably to *Allocation*₁, which is reasonable since most samples in this dataset contain only two images. These results validate the effectiveness of our design.

Setting	ActPred	CFInfer	MoveDir	ObjExist	OCR-VQA
<i>Allocation</i> ₁	53.0	22.0	23.5	42.0	4.5
<i>Allocation</i> ₂	54.5	24.0	23.5	45.0	3.5
Ours	56.0	25.0	25.5	47.0	4.5

Table 6: Performance comparison across different allocation settings.

G Hyperparameter Analysis

To evaluate the sensitivity of our method to hyperparameters, we examine three different configurations, including the first stage token budget bounds (M_{min}, M_{max}), the candidate budget M_2 and the scaling factor λ . Specifically, *Hyper*₁ ($M_{min} = 294, M_{max} = 454, M_2 = 252, \lambda = 0.5$) represents a high variance setting, where the token budget is heavily influenced by the factor s . In contrast, *Hyper*₃ ($M_{min} = 374, M_{max} = 454, M_2 = 317, \lambda = 0.2$) corresponds to a conservative strategy, featuring a higher minimum budget and reduced sensitivity to scaling. *Hyper*₂ ($M_{min} = 334, M_{max} = 374, M_2 = 226, \lambda = 0.3$) serves as an intermediate configuration, balancing the two extremes. We implement these three configurations on LLaVA-1.5-7B with a token retention rate of 0.3. As shown in Table 7, the results exhibit

only minor differences across these configurations. Our method consistently achieves stable and strong performance under all settings, further demonstrating its robustness to variations in hyperparameters.

Setting	ActPred	CFInfer	MMQA	ObjExist	OCR-VQA
<i>Hyper</i> ₁	55.0	17.5	62.0	48.0	8.5
<i>Hyper</i> ₂	55.0	17.5	61.0	49.0	8.5
<i>Hyper</i> ₃	55.5	17.0	60.0	48.0	9.0

Table 7: Performance on LLaVA-1.5-7B under different hyperparameter settings.

H Implementation Details

Our experiments are conducted using the PyTorch framework (Paszke et al., 2019) and the Hugging Face Transformers library (Wolf, 2020). We utilize an NVIDIA H100 GPU with 80GB of memory. We adopt accuracy as the evaluation metric for ActionPrediction (ActPred), CounterfactualInference (CFInfer), MovingDirection (MoveDir), MultiModalQA (MMQA), ObjectExistence (ObjExist), ObjectShuffle (ObjShuf) and OCR-VQA, while Rouge-L is used to evaluate the ALFRED and IEdit datasets. Our evaluation also includes some shorter multi-image datasets, such as OCR-VQA, where the number of images is typically 2 to 3. We evaluate our method across multiple datasets and find that the values of s (Eq. 8) mostly lie in the range of 1 to 2. We set the default values of the parameters $M_{min}, M_{max}, \lambda$ and M_2 to 294, 454, 0.5 and 252, respectively. We also conduct a hyperparameter analysis, which shows that satisfactory performance can be achieved across different hyperparameter settings. We set the token retention ratio to 0.2 in both the comparative and ablation experiments.

I Pruning Analysis

Analysis of Pruned Regions We analyze the visual token pruning behavior under long context inputs and find that this method tends to prune regions that are highly redundant within a single image, semantically low-density, and repeatedly appear across multiple images, such as large background areas, repetitive textures, and local regions with minimal variation between adjacent images. These regions exhibit high similarity in the feature space and contribute little additional semantic information, and are therefore prioritized for compression. In contrast, regions that are semantically irreplaceable are more likely to be retained, including those that capture the core structural content of an image, regions exhibiting significant changes across images, and local visual cues that are strongly aligned with the textual context. Such regions are more widely dispersed in the embedding space and play a more crucial role, which in turn leads to their preferential retention in the final multi-image visual representation.

Performance on Challenging Samples Our evaluation dataset contains a large number of highly challenging samples, such as inputs with vague and semantically sparse textual descriptions (e.g., ‘‘Please provide a common theme for these input images’’), as well as images in which the key semantic elements occupy only a very small region. Strong performance on these benchmarks demonstrates that our method can robustly preserve critical visual information and maintain reliable reasoning capabilities even under such difficult input conditions.

Evaluation over Multiple Runs Under the evaluation framework adopted in this work and the runtime environment described in the paper, the execution of the model is fully deterministic. As a result, repeated runs under the same settings do not introduce any randomness or variability in the outcomes. We conducted multiple independent runs using identical configurations, and the results were completely consistent across all trials, with no observable fluctuations in any of the reported metrics. This confirms that the reported performance is stable and reproducible under the specified experimental conditions.

J Acceleration Details

To compute the diversity metric $\mathcal{D}_{intra}(I)$, directly enumerating all token pairs incurs quadratic computational cost. We therefore reformulate it into an equivalent linear form. Let the normalized visual tokens of image I be $\{x_i^{(I)}\}_{i=1}^N$, and define the aggregate representation as follows:

$$S_I = \sum_{i=1}^N x_i^{(I)} \quad (20)$$

Using the identity, we obtain the following expressions:

$$\|S_I\|^2 = \langle S_I, S_I \rangle = \left\langle \sum_{i=1}^N x_i^{(I)}, \sum_{j=1}^N x_j^{(I)} \right\rangle \quad (21)$$

$$\|S_I\|^2 = \sum_{i=1}^N \|x_i^{(I)}\|^2 + \sum_{i \neq j} \langle x_i^{(I)}, x_j^{(I)} \rangle \quad (22)$$

Due to our normalization of these vectors, we obtain the following formula:

$$\sum_{i=1}^N \|x_i^{(I)}\|^2 = \sum_{i=1}^N 1 = N \quad (23)$$

$$\sum_{i \neq j} \langle x_i^{(I)}, x_j^{(I)} \rangle = \sum_{i \neq j} \cos(x_i^{(I)}, x_j^{(I)}) \quad (24)$$

Therefore, $\|S_I\|^2$ can be expressed as follows:

$$\|S_I\|^2 = N + \sum_{i \neq j} \cos(x_i^{(I)}, x_j^{(I)}) \quad (25)$$

The original pairwise definition is given as follows:

$$D_{intra}(I) = \frac{1}{N(N-1)} \sum_{i \neq j} (1 - \cos(x_i^{(I)}, x_j^{(I)})) \quad (26)$$

Based on the above derivation, it can be reformulated as follows:

$$D_{intra}(I) = \frac{N(N-1) - (\|S_I\|^2 - N)}{N(N-1)} \quad (27)$$

Similarly, the token diversity score v_i can be rewritten as follows:

$$v_i = \frac{N - (x_i^{(I)})^\top S_I}{N-1} \quad (28)$$

These reformulations yield exactly the same value as the original definition, while avoiding explicit pairwise computation and reducing the complexity

from $O(N^2)$ to $O(N)$. For instance, at a sequence length of 8192, it incurs only 2.88 ms of overhead and achieves a $23.65 \times$ speedup.

When computing the alignment score between visual tokens and text tokens, let N_v denote the number of visual tokens, M the number of text tokens, and d the feature dimension of each token. A naive implementation directly computes the squared distance between each visual token and all text tokens and then averages the results, resulting in a complexity of $O(N_v \cdot M \cdot d)$. This becomes computationally expensive when either the number of visual tokens or the feature dimension is large. To improve efficiency, we exploit the algebraic expansion of the squared distance:

$$|x_i - t_j|^2 = |x_i|^2 + |t_j|^2 - 2x_i^\top t_j \quad (29)$$

Thus, the alignment score for each visual token x_i can be rewritten as follows:

$$a_i = -|x_i|^2 - C + 2x_i^\top \mu_t \quad (30)$$

where $\mu_t = \frac{1}{M} \sum_j t_j$ and $C = \frac{1}{M} \sum_j |t_j|^2$ are pre-computed constants. This formulation is mathematically equivalent to the naive implementation and introduces no approximation. By expanding the formula, we avoid constructing a large $[N_v, M, d]$ tensor and computing each visual-text pair individually. Instead, we only need to perform a single sum or squared sum over the text tokens and a vector dot product and norm computation for each visual token. This reduces the computational complexity from $O(N_v \cdot M \cdot d)$ to $O((N_v + M)d)$, significantly accelerating computation when the number of visual tokens or the feature dimension is large while maintaining exact numerical equivalence. For example, when $N_v, M = 8192, 128$, it achieves a $1.3 \times$ speedup.

In our pareto selection implementation, to improve computational efficiency, since only two objectives are involved, this process can be efficiently realized via a sorting and scanning strategy instead of exhaustive pairwise comparisons. Specifically, all candidate solutions are first sorted in descending order according to the first objective f_1 . Then, we perform a single linear scan while maintaining the maximum value of the second objective f_2 observed so far. A candidate is selected as a pareto optimal solution if its f_2 value exceeds the current maximum, indicating that it is not dominated by any previously considered solution. This process yields the pareto front in $O(N \log N)$ time due to

sorting, followed by an $O(N)$ scan. Moreover, this process occurs in the final step, at which point the number of tokens is already reduced and N is relatively small. For example, when $N = 500$ and the selected size is 14, it achieves a $14.76 \times$ speedup.

K Case Study

To qualitatively evaluate the effectiveness of our pruning strategy, we conduct a case study on several representative samples using LLaVA-1.5-7B. Figure 4 presents illustrative examples that highlight the adaptive behavior of our method. For sequential tasks involving object interactions, our approach leverages image variations to effectively filter redundant information from static backgrounds, thereby allocating the limited token budget to dynamic foreground entities. As a result, the model can accurately identify critical objects even under highly compressed visual representations. In the query case related to the Scottish League Cup, the diversity metric ensures that nuanced, semantically important details such as text and logos are preserved. Overall, these results demonstrate that our method can effectively distinguish redundant visual content from semantically salient signals.

Based on the provided images, answer the question related to the moving attribute. You must choose your answer from the Choice List.
 <ImageHere>...<ImageHere>
 What is the material of the stationary cylinder when the video ends?
 Choice list:
 A. rubber
 B. metal
 Your answer is:

 GT: Rubber.
 Predict: A.



(a)

The team with a logo that is circular in shape, among away team in Second round of 1995-96 Scottish League Cup, is?
 <ImageHere>...<ImageHere>
 Choice list:
 A. Heart of Midlothian F.C.
 B. Hibernian F.C.
 C. Dundee United F.C. Motherwell F.C. Hamilton Academical F.C. Partick Thistle F.C. Falkirk F.C. Stenhousemuir F.C. St Mirren F.C. Celtic F.C.
 D. Greenock Morton F.C.
 Your answer is:

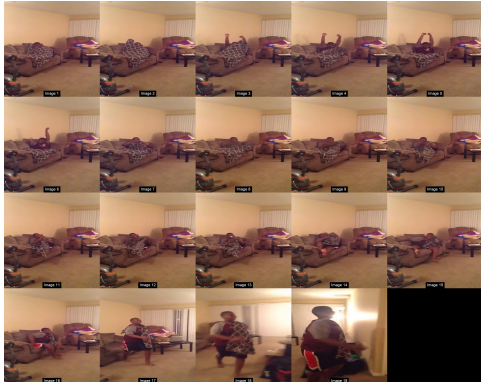
 GT: The Dundee United F.C. Motherwell F.C. Hamilton Academical F.C. Partick Thistle F.C. Falkirk F.C. Stenhousemuir F.C. St Mirren F.C. Celtic F.C.
 Predict: C.



(b)

Based on the provided images, answer the question related to the interaction of objects. You must choose your answer from the Choice List.
 <ImageHere>...<ImageHere>
 Which object was taken by the person?
 Choice list:
 A. The dish.
 B. The box.
 C. The blanket.
 D. The paper/notebook.
 Your answer is:

 GT: The blanket.
 Predict: C.



(c)

Which object was tidied up by the person?
 <ImageHere>...<ImageHere>
 Choice list:
 A. The table.
 B. The towel.
 C. The broom.
 D. The closet/cabinet.
 Your answer is:

 GT: The closet/cabinet.
 Predict: D.



(d)

Figure 4: Case study of our pruning strategy on several LLaVA-1.5-7B samples. GT denotes Ground Truth.